Molecular driving forces defining lipid positions around aquaporin-0

Camilo Aponte-Santamaría[a], Rodolfo Briones[a], Andreas D. Schenk[b], Thomas Walz[b,c], and Bert L. de Groot[a,1]

[a]Department of Theoretical and Computational Biophysics, Max Planck Institute for Biophysical Chemistry, Göttingen, Germany; [b]Department of Cell Biology, and [c]Howard Hughes Medical Institute, Harvard Medical School, Boston, MA 02115

Edited by Wolfgang Baumeister, Max-Planck-Institute of Biochemistry, Martinsried, Germany, and approved May 4, 2012 (received for review December 22, 2011)

Lipid–protein interactions play pivotal roles in biological membranes. Electron crystallographic studies of the lens-specific water channel aquaporin-0 (AQP0) revealed atomistic views of such interactions, by providing high-resolution structures of annular lipids surrounding AQP0. It remained unclear, however, whether these lipid structures are representative of the positions of unconstrained lipids surrounding an individual protein, and what molecular determinants define the lipid positions around AQP0. We addressed these questions by using molecular dynamics simulations and crystallographic refinement, and calculated time-averaged densities of dimyristoyl-phosphatidylcholine lipids around AQP0. Our simulations demonstrate that, although the experimentally determined crystallographic lipid positions are constrained by the crystal packing, they appropriately describe the behavior of unconstrained lipids around an individual AQP0 tetramer, and thus likely represent physiologically relevant lipid positions.While the acyl chains were well localized, the lipid head groups were not. Furthermore, in silico mutations showed that electrostatic inter actions do not play a major role attracting these phospholipids towards AQP0. Instead, the mobility of the protein crucially modulates the lipid localization and explains the difference in lipid density between extracellular and cytoplasmic leaflets. Moreover, our simulations support a general mechanism in which membrane proteins laterally diffuse accompanied by several layers of localized lipids, with the positions of the annular lipids being influenced the most by the protein surface. We conclude that the acyl chains rather than the head groups define the positions of dimyristoyl-phosphatidylcholine lipids around AQP0. Lipid localization is largely determined by the mobility of the protein surface, whereas hydrogen bonds play an important but secondary role.

electron crystallography | lipd bilayer | atomistic simulations

Lipids and membrane proteins form biological membranes that constitute the boundary of cells and their intracellular compartments. Lipids arrange in a bilayer conformation that serve as a 2D fluid for membrane proteins. The lipid bilayer, however, is more than a passive fluid and influences many aspects of membrane proteins, including their insertion into the membrane (1, 2), assembly into complexes (3–5), and activity (6, 7). Conversely, membrane proteins alter the conformational properties of lipid bilayers, mediating for instance pore formation (8), fusogenicity (9), and membrane bending (10, 11). Detailed knowledge of how lipids and membrane proteins interact with each other is therefore crucial to understand the molecular machinery of biological membranes.

To date, spectroscopic methods have contributed most to our understanding of lipid–protein interactions, providing insight into the dynamics of such interactions (1, 12). Atomistic views were obtained by structures of membrane proteins either with few specifically bound lipids or surrounded by a complete ring of lipids, determined by X-ray (13–17) and electron crystallography (18–20). Furthermore, molecular dynamics (MD) and coarse-grained simulations have added a wealth of dynamic and energetic information creating a better understanding of the principles underlying lipid–protein interactions (for comprehensive reviews see refs. 21 and 22).

Electron crystallographic studies of the lens-specific water channel aquaporin-0 (AQP0) have emerged as a promising approach for systematic structural studies of lipid–protein interactions (19, 20, 23–27). Electron crystallography uses 2D crystals of membrane proteins reconstituted into artificial lipid bilayers and thus allows the structure of membrane proteins to be determined in their native environment (24, 25, 28). The 1.9-Å structure of AQP0 crystallized in dimyristoyl-phosphatidylcholine (DMPC) revealed not only the protein, but also the first shell of lipids, called the annular lipids, surrounding the AQP0 tetramers (19). The structure of the complete ring of annular lipids defined the preferred lipid positions around the protein and provided insights into the nature of nonspecific lipid–protein interactions. Moreover, the annular lipids were also observed in the recent 2.5-Å structure of AQP0 crystallized in *Escherichia coli* polar lipids (20), demonstrating that high-quality 2D crystals of AQP0 can be produced with different lipids.

The electron crystallographic structures of AQP0 raised several questions: Are the observed crystallographic lipid structures, which correspond to lipids sandwiched in between two tetramers in the 2D crystals, representative of the positions adopted by unconstrained lipids surrounding a single AQP0 tetramer? What are the molecular driving forces stabilizing the observed lipid positions around AQP0? How does AQP0 affect lipids beyond the first annular layer? We addressed these questions by using MD simulations and crystallographic refinement. We calculated time-averaged density maps of DMPC bilayers either surrounding an individual AQP0 tetramer or constrained by four AQP0 tetramers simulating the situation in a 2D crystal.

Results

Lipid Arrangement Around a Single AQP0 Tetramer. We first performed 100-ns MD simulations of a single AQP0 tetramer embedded in a DMPC bilayer (Fig. 1*A*, *Left*, and *SI Appendix*, Fig. S1) and calculated a time-averaged lipid-density map ρ around the tetramer (in the following called MD map). Because each monomer in the AQP0 tetramer has identical lipid interfaces, composed of surfaces S1 and S2 (Fig. 1*A*), we fourfold symmetrized the map to produce the average lipid density around a single AQP0 monomer, which we could compare with the lipids seen in the electron crystallographic structure of AQP0 (19) (Fig. 1*B*).

For most of the crystallographic lipids (labeled PC1–PC7), portions of their tails fall into high-density regions of the MD map. In particular, almost the entire tails of lipid PC1 in the

Author contributions: C.A.S., R.B., A.D.S., T.W., and B.L.d.G. designed research, performed research, analyzed data, and wrote the paper.

The authors declare no conflict of interest.

This article is a PNAS Direct Submission.

[1]To whom correspondence should be addressed. E-mail: bgroot@gwdg.de.

This article contains supporting information online at www.pnas.org/lookup/suppl/doi:10.1073/pnas.1121054109/-/DCSupplemental.

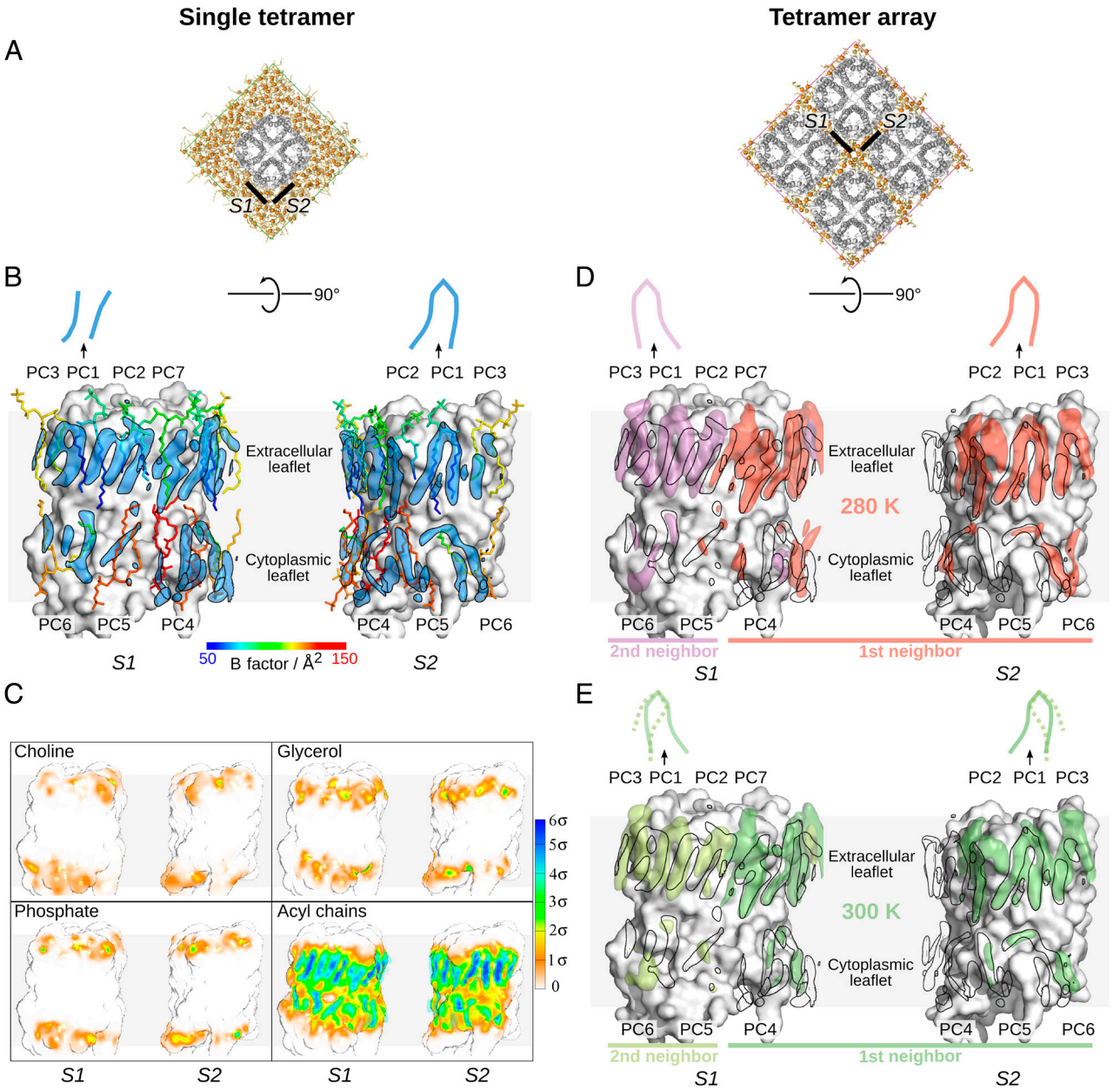

Fig. 1. Time-averaged lipid-density maps around AQP0 obtained from MD simulations. (*A*) Top views (perpendicular to the membrane plane) of a single AQP0 tetramer embedded in a DMPC lipid bilayer (*Left*) and an array of four AQP0 tetramers with sandwiched DMPC molecules (*Right*). AQP0 tetramers are shown in white and DMPC lipids in orange and yellow. S1 and S2 indicate the two lipid-facing surfaces of an AQP0 monomer. *B*–*E* show side views of surfaces S1 and S2 indicated in *A*. (*B*) Comparison between the DMPC molecules seen in the electron crystallographic structure of AQP0 (19) and the lipid-density map obtained from an MD simulation of an AQP0 tetramer inserted into an equilibrated DMPC patch (*A*, *Left*). The crystallographic lipids, labeled PC1 to PC7, are shown in stick representation and color-coded according to their B factor (color scale at the bottom). The MD-derived density map is contoured at 4σ and shown as blue surface enclosed by black lines. (*C*) Contributions of different lipid groups to the MD-derived lipid-density map shown in *B*. The density map at a distance of 5.6 Å from the protein is depicted according to the scale at the right side. (*D*–*E*) Lipid-density maps obtained from MD simulations of a system containing an array of four AQP0 tetramers in a 2D crystal arrangement (*A*, *Right*), at 280 (*D*) and 300 K (*E*). Maps were contoured at 3.2σ. For comparison, the density map obtained from the simulation with a single tetramer (*B*) is shown as black contours. The sketches on top represent the major conformations sampled during the simulations by the lipids at the position of crystallographic lipid PC1.

extracellular leaflet at surface S2 are represented by high density in the computed map. The middle part of lipid PC3 at S1 and one of the tail ends of lipid PC3 at S2 also coincide with high-density regions in the MD map, which also captures the separation of the tails of lipid PC6 at S1. In addition, the MD map shows a favorable degree of correlation with the crystallographic B factors of the lipids: Portions of the lipids with low B factors (less positional uncertainty) match with high-density regions, and portions of the lipids with high B factors (more positional uncertainty) correspond to regions of weak density. Remarkably, two independent simulations of a single tetramer, either including the crystallographic lipids or inserted into an equilibrated lipid patch (*SI Appendix*, Fig. S1*A*), produced similar density maps (*SI Appendix*, Fig. S2). Moreover, shortening the production runs to only 50% of the simulation length (50 ns) did not induce substantial changes in the density maps (*SI Appendix*, Fig. S3). These two results indicate convergence of the lipid positions on the simulated timescale. Unless stated otherwise, the MD map obtained with a single AQP0 tetramer inserted into a DMPC patch (without the crystallographic lipids) was used for all further analysis.

To further analyze the MD map, we inspected the contributions made by the different parts of the lipids (Fig. 1*C*). High-density values ($\rho > 4\sigma$), corresponding to more localized positions during the simulations, are mainly observed for the acyl chains, whereas the densities representing the head groups (choline, phosphate, and glycerol) are found to be weak ($\rho < 3\sigma$).

In addition, the MD map revealed an asymmetry between the two leaflets regarding the number of well-defined tail positions (Fig. 1*B*). Eleven well-defined tail positions are observed in the extracellular leaflet and only six in the cytoplasmic leaflet. Moreover, the density is much weaker in the cytoplasmic leaflet than in the extracellular leaflet. The asymmetry is also reflected in the computed deuterium parameters, which show different average tilting angles (with respect to the axis normal to the membrane) for the acyl chains of annular lipids in the extracellular leaflet compared to those in the cytoplasmic leaflet (*SI Appendix*, Fig. S4 *A* and *B*).

Effect of Crystal Packing on the Lipid Positions. To investigate the effect of the dense protein packing in the 2D crystals on the positioning of the annular lipids surrounding AQP0, we performed MD simulations with lipids sandwiched between four tetramers in the crystal packing arrangement (Fig. 1*A*, *Right*, and *SI Appendix*, Fig. S1*B*) at two different temperatures, 280 and 300 K.

To calculate the time-averaged lipid-density map, each lipid molecule was assigned to its closest AQP0 monomer (labeled first neighbor in Fig. 1 *D* and *E*). In the resulting density maps, high-density regions are mainly located near surface S2 (Fig. 1 *D* and *E*). High-density regions in these tetramer-array maps colocalize with those in the single-tetramer map on surface S2, with the best-defined position observed at the place of crystallographic lipid PC1. Nevertheless, the density at the position of crystallographic lipid PC3 is stronger in the tetramer-array maps than in the single-tetramer map (see also differences in *SI Appendix*, Fig. S5), indicating that this lipid is more strongly localized in the context of a crystalline array than when associated only with a single AQP0 tetramer. In addition, the deuterium parameters were found to be in a broader range of values for the acyl chains of lipids sandwiched in between AQP0 tetramers than for the acyl chains of lipids surrounding an individual tetramer (compare *SI Appendix*, Fig. S4 *C* and *D* with Fig. S4 *A* and *B*).

Interestingly, the tetramer-array maps revealed that lipids at crystallographic position PC1 adopt primarily one conformation in the simulation at 280 K (Fig. 1*D*) and alternate between two conformations in the simulation at 300 K (Fig. 1*E*). The single conformation in the 280 K map matches the conformation seen on surface S2 in the single-tetramer map, but deviates from the conformation seen on surface S1, as observed when the tetramer-array map is projected onto surface S1 by assigning the lipid positions to the second-closest (second neighbor) AQP0 monomer (compare Fig. 1*D* with Fig. 1*B*). In contrast, the 300 K map displays two conformations: The first one matches the one seen on surface S1 in the single-tetramer map, and the second corresponds to the one seen on surface S2 in the single-tetramer map (compare Fig. 1*E* with Fig. 1*B*).

Refinement of Lipid Structures Based on Lipid-Density Maps Derived from MD Simulations. Although the MD map shows many similarities with the electron crystallographic structure, there are also numerous differences in lipid conformations. To assess whether these differences constitute inconsistencies between the MD-derived and the crystallographic datasets or represent alternative lipid conformations, we modeled lipids into the MD density and then refined them against the electron crystallographic data (19) (Fig. 2). Refinement did not affect the positions of the acyl chains and glycerol backbone of lipid PC1, but parts of the remaining lipids moved to slightly different positions (Fig. 2, *Left*). The refined structure includes five complete lipids in the extracellular leaflet and four in the cytoplasmic leaflet, and both leaflets also contain a single acyl chain near the fourfold axis. In comparison to the original structure, the MD map allowed identification of an additional acyl chain in the extracellular leaflet (PC11) and an additional full lipid in the cytoplasmic leaflet (PC10).

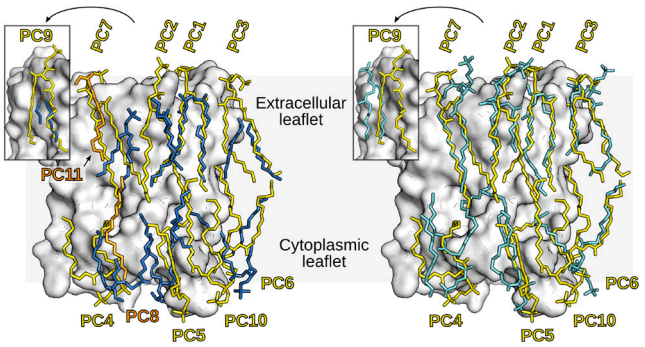

Fig. 2. Refinement of lipid structures around AQP0 by using MD and electron crystallography data. The lipid moieties modeled into the density map derived from the MD simulation of a single tetramer (presented in Fig. 1*B*) are shown in blue. The lipids after refinement against the electron crystallography data (19) are presented in yellow (complete lipids) and orange (individual acyl chains). The original crystallographic lipids (19) are shown in cyan for comparison. The AQP0 monomer is shown in surface representation. For clarity, lipid PC9 is depicted separately in the insets, and the individual acyl chains PC8 and PC11 are not shown in the right figure.

The lipids in the refined structure based on the MD map show many similarities with those in the original crystallographic structure, especially those in the extracellular leaflet, PC1, PC2, PC3, and PC7 (Fig. 2, *Right*), but there are also some local differences. For example, one acyl chain of lipid PC1, which shows the best-defined density in all datasets, has a bent conformation in the MD map but has a more straight conformation in the crystallographic structure. Moreover, lipid PC9 is not in direct contact with the protein surface in the original crystallographic structure, but it is in contact in the MD map. The refined structure also exhibits a different orientation for the two hydrogen bond-forming protein residues Arg113 and Arg196 (*SI Appendix*, Fig. S6*D*).

In addition to this converged MD map, we also used a nonconverged MD simulation (100-ps length) as a control. The lipids modeled into the nonconverged density map matched neither the lipid positions in the converged MD map nor in the original crystal structure (*SI Appendix*, Fig. S6 *E* and *F*). However, upon refinement against the crystallographic data, the lipids modeled into the nonconverged map exhibited big shifts (especially in the first refinement steps) and finally approached the same positions as those seen in the converged model after refinement (compare *SI Appendix*, Fig. S6*C* with Fig. S6*G*, and see further details in the *SI Appendix*).

Strong Protein-Lipid Interaction Sites and in Silico Mutations. We monitored the potential energy between lipids and AQP0 during the MD simulations (Fig. 3*A*), and thereby identified seven residues at the AQP0 surface that strongly interact with lipids: R5, Y105, R113, R196, and K238 through electrostatic interactions, and W10 and W202 through van der Waals interactions (see also *SI Appendix*, Fig. S7*A*). Correlation between the Coulomb interaction energy and the presence of hydrogen bonds suggests that the electrostatic residue-lipid interactions are mediated by hydrogen bonds (*SI Appendix*, Fig. S7*B*). In the extracellular leaflet, the side chain of R196 forms up to four hydrogen bonds, for more than half of the simulation time, mainly with the carboxyl and phosphatidyl-ester oxygens (*SI Appendix*, Fig. S7*C*) of lipids at positions PC1, PC2, and PC7 (*SI Appendix*, Fig. S7*D*). The neighboring residues Y105 and R113 form hydrogen bonds with lipids at positions PC1 and PC3, but less frequently than R196. Similar

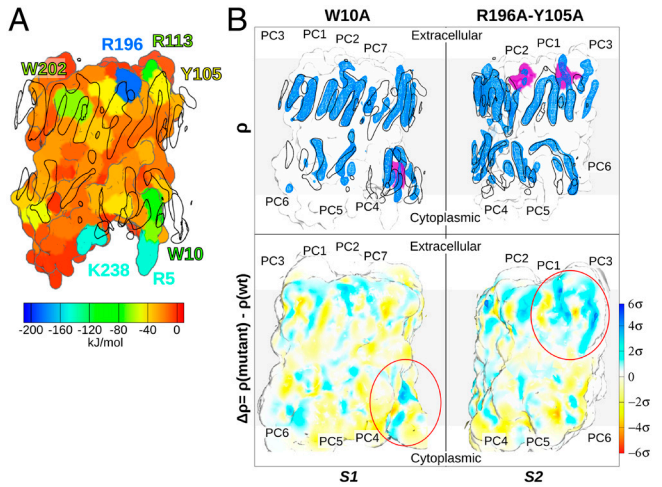

Fig. 3. Interaction energy between the lipids and AQP0 computed from MD simulations. (*A*) Time-averaged potential interaction energy derived from a simulation of a single AQP0 tetramer embedded in a DMPC lipid bilayer. The energy is depicted in color representation according to the scale at the bottom. Labels correspond to AQP0 residues strongly interacting with lipids, either through electrostatic (R5, Y105, R113, R196, and K238) or van der Waals (W10 and W202) interactions. High lipid-density regions (presented in Fig. 1*B*) contoured at 4σ are outlined in black. (*B*) Effects of mutating AQP0 residues that strongly interact with lipids on the resulting MD-derived lipid-density maps. Two representative maps, obtained with the W10A and the R196A-Y105A mutations, are shown (see *SI Appendix*, Figs. S8–S10 for all 12 maps). The *Top* panels show the mutated residues in purple and the resulting lipid-density maps contoured at 4σ as blue mesh. For comparison, the lipid-density map obtained with wild-type AQP0 contoured at 4σ is displayed as black contours. The lower panels depict differences between the lipid-density maps obtained with mutant and wild-type AQP0 (see scale for color coding). The red circles indicate regions with an increase in lipid-density near the mutated residues.

to R196 in the extracellular leaflet, the side chains of R5 and K238 in the cytoplasmic leaflet also make intermittent hydrogen bonds mainly with carboxyl and ester oxygens of the annular lipids.

To test whether these strongly interacting residues constitute phospholipid-binding sites, we performed MD simulations in which we mutated them to alanine: 10 simulations of 100 ns each, including single, double, and triple mutations. Changes in the lipid-density around AQP0 mutants are in the range from 1σ to 2σ. Larger changes in the density map primarily correspond to lipid atoms occupying space freed by deletion of the side-chains of the mutated residues (Fig. 3*B*, *Right*, and *SI Appendix*, Figs. S8 and S9). Compared to wild-type AQP0, the mutations did not substantially modify the lipid positions, and the well-defined tail positions were always observed throughout all mutant simulations.

The Effect of Protein Mobility on the Lipid Positions. Calculation of the rms fluctuations (RMSF) in the MD trajectories revealed that the protein surface displays a wide range of flexibility (Fig. 4*A*). Residues in transmembrane helices (especially those close to the extracellular surface of the protein) are mostly rigid, whereas the N and C termini are highly flexible. Despite their strong electrostatic interactions, residues R5, R196, and K238 are also very mobile. Overall, we found that the RMSF are positively correlated with the crystallographic B factors of the protein (19) (*SI Appendix*, Fig. S11).

To analyze the relation between protein mobility and lipid density, we defined F as the fraction of a cylinder (of radius 7.5 Å and height 4 Å) that is occupied by high lipid-density points ($\rho > 4\sigma$), and plotted this quantity as a function of the RMSF of the protein atom centered in the cylinder (Fig. 4*B*). Near high-RMSF atoms, such as the ones in the flexible N and C termini, F invariably takes

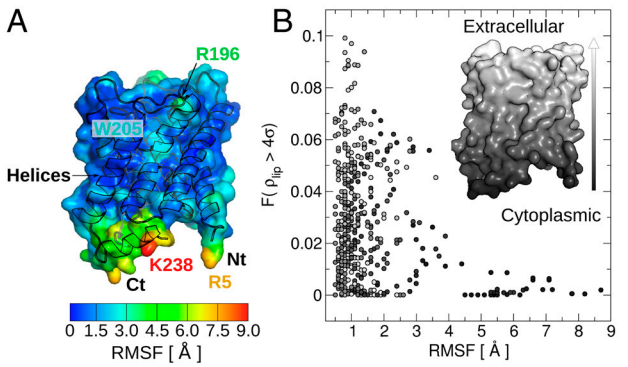

Fig. 4. Effect of AQP0 mobility on lipid positions. (*A*) RMSF derived from MD simulations are shown as a measure of the flexibility of the protein surface. The RMSF are color-coded according to the scale at the bottom. (*B*) F defined as the fraction of a cylinder (of radius 7.5 Å and height 4 Å) occupied by high lipid-density points ($\rho > 4\sigma$) plotted as a function of the RMSF of the surface atom centered in the cylinder. The gray scale represents the position of the atom along the coordinate normal to the membrane (as illustrated in the inset).

on small values. In contrast, in the vicinity of low-RMSF atoms, F displays a broader range of values, thus allowing highly localized lipid positions.

Lipid Behavior Distant from AQP0. An analysis of the behavior of lipids distant from the protein (Fig. 5 and *SI Appendix*, Fig. S12) revealed that only the annular lipids display strong density regions, whereas with increasing distance from the protein the lipid density rapidly weakens and becomes "bulk-like." However, at intermediate distances (a few lipid shells away from AQP0), the lipids still show a moderately localized behavior. Very different density patterns are observed for the two leaflets. For instance, at the height of the tips of the acyl chains, the map presents stronger densities in the extracellular leaflet than in the cytoplasmic leaflet. In contrast, at the height of the head groups (both glycerol and phosphate), the density is predominantly higher in the cyto-

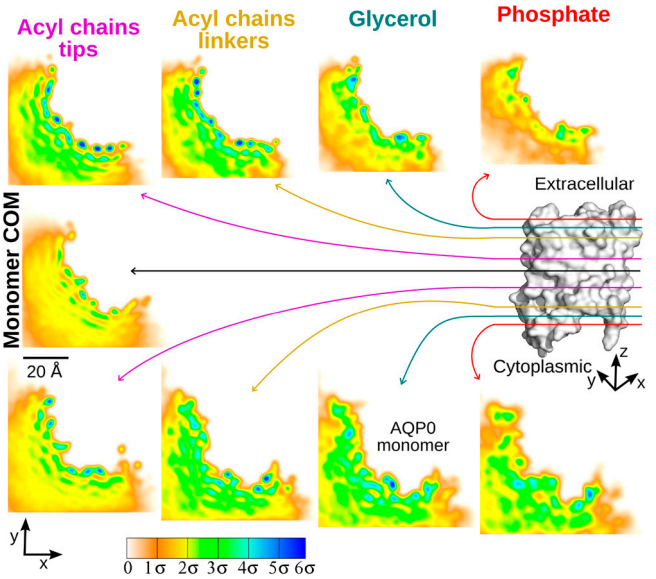

Fig. 5. Lipid density around an AQP0 monomer beyond the annular lipid shell, recovered from the simulation of a single tetramer embedded in a DMPC lipid bilayer without the crystallographic lipids (see *SI Appendix*, Fig. S12 for simulations with and without the crystallographic lipids). The color maps represent lateral projections (onto the *xy* membrane plane) of the lipid density, at the different *z* positions indicated on the AQP0 monomer (white). Projections were taken at the average *z* positions of the center of masses (COM) of the indicated lipid groups (for both leaflets, upper and lower maps) and the AQP0 monomer (middle map).

plasmic leaflet compared to that in the extracellular leaflet. This finding indicates that the effect of leaflet asymmetry (noted before for annular lipids) extends to lipids distant from the protein.

Discussion

Lipids in AQP0 2D Crystals Behave Similarly to Lipids Surrounding a Single AQP0 Tetramer. Our results demonstrate that the majority of lipid structures and their B factors seen by electron crystallography of AQP0 2D crystals are representative of the average positions adopted by unconstrained lipids surrounding an individual AQP0 tetramer seen in the MD map (Fig. 1*B*). Nevertheless, lipids sandwiched in between AQP0 tetramers have a stronger degree of alignment than lipids only in contact with a single AQP0 tetramer, as reflected in the calculation of the deuterium order parameters (*SI Appendix*, Fig. S4).

The favorable agreement between the computed lipid-density maps and the crystallographic structures also provides an independent validation of the used lipid and protein simulation parameters (force field). Moreover, the similarity of the lipid-density maps obtained in two independent simulations (*SI Appendix*, Fig. S2) indicates that lipids adopt stable positions around AQP0 in a timescale of tens of nanoseconds, and independent of their initial positions.

Our simulations reveal that the acyl chains are the most localized parts of annular lipids, generating strong density in the time-averaged map, whereas the lipid head groups are less localized and thus create only weak density (Fig. 1*C*). This result supports the hypothesis deduced from electron crystallographic structures, that acyl chains are mainly responsible for stabilizing the saturated DMPC lipids around AQP0, whereas the head groups make only a secondary contribution to lipid localization (20). Electron crystallography also revealed that acyl chains of unsaturated *Escherichia coli* polar lipids occupy similar positions as those of the saturated DMPC lipids (20), thus suggesting that acyl chains play an important stabilizing role not only for saturated but also for unsaturated lipids.

Our simulations also show that the lipids in the 2D crystal accommodate closer to protein surface S2 of a tetramer than to S1 of their adjacent tetramer, suggesting that S2 mostly defines the lipid positions in the crystal (Figs. 1 *D* and *E*). This effect can be attributed to the observed strong electrostatic interactions between the lipids and residues R196, Y105, and R113 (extracellular leaflet), and R5 (cytoplasmic leaflet), all of which are located at surface S2 (Fig. 3*A*). The lack of electrostatic interactions with residues at S1 may also explain why high-density contours in the MD map (resulting from stable lipid positions) and the positions of the crystallographic lipids do not match as well at S1 as they do at S2.

Lipids at the crystallographic position PC1 were found to adopt two conformations at 300 K, when located in the crystal environment. Each conformation matches one of the two conformations adopted by lipids at position PC1 around an isolated AQP0 tetramer facing either surface S1 or S2 of the monomer (Fig. 1*E*). This result thus suggests that the lipid at this position in the 2D crystal, sandwiched between surfaces S1 and S2, alternates between two conformations at 300 K, and also illustrates how the lipid conformations may be influenced by the surface of the protein. When the temperature was decreased to 280 K, only one of the two conformations was sampled (Fig. 1*D*). At the very low temperature at which the electron crystallographic data were collected, the lipids would be expected to only adopt this conformation, which was indeed the case.

Refinement of Crystallographic Lipid Positions Validates the MD Data. When lipids were built into the MD map and subsequently refined against the electron crystallographic data, annular lipid PC1 in the extracellular leaflet retained its position, and the refined structures matched the original crystallographic lipid structures (Fig. 2 and *SI Appendix*, Fig. S6). When, as a control, the lipids were deliberately built into a nonconverged MD map, refinement against the electron crystallographic data moved the lipids close to the crystallographic positions (*SI Appendix*, Fig. S6). These results underscore the validity of the MD-derived density maps and show that the refined structures are not strongly biased by the initial model. In addition, they reveal that the lipids adopt preferred positions around AQP0 not only in the context of a 2D crystal but that they use similar positions when surrounding an individual AQP0 tetramer.

AQP0 Does Not Have Specific Phospholipid-Binding Sites. Strong electrostatic protein–lipid interactions—mediated by hydrogen bonds—suggested the possibility that Y105, R113, and R196 at the extracellular leaflet, and R5 and K238, at the cytoplasmic leaflet, correspond to phospholipid-binding sites that drive the lipids into the positions observed in both simulations and experiments (Fig. 3*A*). However, these residues did not form stable hydrogen bonds with a specific lipid, but rather transient bonds with all the lipids in their vicinity. The transient nature of the hydrogen bonds is also reflected in the different conformations of the involved protein residues in the refined structures (*SI Appendix*, Fig. S6*D*) and also in their high mobility (Fig. 4*A*). Moreover, in silico mutations of these residues to alanine did not appreciably change the well-defined positions of the lipid tails, in 10 independent simulations with AQP0 mutants spanning a total time of 1.0 μs (Fig. 3*B*, *Right*, and *SI Appendix*, Figs. S8 and S9). Our simulations thus dispose of electrostatic interactions as the main cause that defines the positions of phospholipids around AQP0, and corroborate the conclusion from the electron crystallographic AQP0 structures (20) that residues R196 and Y105 are not part of a phospholipid-binding site as defined by Palsdottir and Hunte (29).

Protein Mobility Interferes with the Localization of Lipids. Our simulations revealed that AQP0 is not a rigid entity but displays a broad range of flexibility. Transmembrane-helix residues at the protein surfaces facing the lipid environment are the most rigid parts, while the N and C termini are highly mobile (Fig. 4*A*). This result is in perfect agreement with the experimental B factors of the protein (19) (*SI Appendix*, Fig. S11). Interestingly, lipid density near the flexible termini was found to be more diffuse compared to the lipid density close to the rigid parts, and only a minor fraction of high-density points was found to reside near highly mobile protein atoms (Fig. 4*B*). Our results thus suggest that mobile segments of the protein interferes with the localization of lipids.

Protein mobility may also provide an explanation for the observed asymmetry in lipid density between the two leaflets (Figs. 1*B* and 5). This asymmetry does not appear to result from lipid immobilization due to protein contacts between the two layers in the double-layered 2D crystals. Instead, it appears that rigid AQP0 residues allow lipids in the extracellular leaflet to be localized, while the flexible termini interfere with localization of lipids in the cytoplasmic leaflet.

Irregularities in the Shape of the Protein Surface Modulate the Lipid Density. Our simulations with AQP0, which has an uneven surface, showed highly localized positions of individual lipid tails for the annular lipids, whereas simulations with transmembrane helices, which have smoother surfaces, did not (30). This result is consistent with the hypothesis by Niemelä et al. that lipid positions in the annular shell are modulated by irregularities in the protein surface (31). Moreover, our MD maps obtained with alanine substitution mutants showed increased lipid density in the space originally occupied by the side chains of the mutated residues (Fig. 3*B* and *SI Appendix*, Figs. S8–S10), illustrating the effect of the shape of the protein surface on lipid arrangement.

An analysis of the protein surface curvature allowed us to distinguish between low curved convex regions (bumps), and highly curved concave areas (clefts) (*SI Appendix*, Fig. S13). Surprisingly, the lipid density did not show a strong correlation with either type of concavity, and high lipid-density points were observed near both concave and convex surface regions. Our curvature calculations therefore support the notion that lipids adapt to the roughness of the exterior surface (bumps or clefts) to form a tight seal around the protein that prevents leakage of solutes across the membrane (for a detailed analysis of the protein surface curvature and concavity see the *SI Appendix*).

AQP0 Influences Lipid Behavior Beyond the First Lipid "Solvation" Shell. In our simulations, lipids only gradually recover their bulk properties with increasing distance from AQP0 (Fig. 5). The protein thus influences not only the localization of the first lipid shell, the annular lipids, but also the following lipid shells. Similar lipid-immobilization patterns have been observed in previous simulation studies with transmembrane helices (30) and ion channels (31). Our results therefore support the model proposed by Niemelä et al. (31), in which the protein forms an obstacle for lateral lipid diffusion perpendicular to the protein surface, thereby influencing the localization of several lipids shells around the protein. Our results, together with these computational studies (30, 31), thus suggest a general mechanism in which membrane proteins laterally diffuse with a highly coordinated lipid solvation shell that consists of several lipid layers, with the positions of the annular lipids being influenced the most by the protein surface.

Conclusions

We used MD simulations and crystallographic refinement to study the localization of DMPC lipids around AQP0. We found that the positions of the constrained lipids in the 2D crystals determined by electron crystallography together with their B factors are representative of the behavior of unconstrained lipids surrounding individual AQP0 tetramers. We conclude that positions of DMPC lipids around AQP0 are defined by the acyl chains rather than the head groups. Furthermore, we observed that the positions of these lipids are largely influenced by the local mobility of the protein, whereas specific hydrogen bonds play a secondary role. Finally, our results are consistent with a general mechanism in which membrane proteins laterally diffuse associated with several layers of lipids, with the positions of the lipids in the first solvation shell being also modulated by irregularities in the protein surface. It will be interesting to investigate if these features are specific for DMPC lipids surrounding AQP0, or rather represent general principles underlying lipid–protein interactions.

Materials and Methods

MD simulations were carried out using the GROMACS 4.0 simulation package (32, 33). Two different systems were simulated (Fig. 1*A* and *SI Appendix*, Fig. S1). The first system consisted of a single AQP0 tetramer embedded in a fully solvated DMPC lipid bilayer, simulating a membrane at low protein concentration. The second system included four densely packed AQP0 tetramers in the 2D crystal arrangement, with DMPC molecules filling the gaps between the tetramers and surrounded by explicit water molecules. The production runs were 100 ns in length and the first 10 ns were excluded to account for equilibration time. Additional simulations with AQP0 mutants (12 in total), in which residues of interest were substituted by alanine, were carried out following the same simulation scheme as for the single-tetramer system. The lipid density around a single AQP0 monomer was time-averaged over a concatenated trajectory consisting of fitted trajectories of individual AQP0 monomers (four in the single-tetramer and 16 in the four-tetramer system) together with their closest surrounding lipids. Additional simulation details, the methods used to calculate the lipid-density maps and other observables from the simulations, and the structure refinement procedure are described in the *SI Appendix*.

ACKNOWLEDGMENTS. We thank Ulrike Gerischer and Dirk Matthes for careful reading of the manuscript. This work was supported by grants from the Max Planck Society (C.A.S. and B.L.d.G.), the European Commission (Marie Curie Research Training Network MRTN-CT-2006-035995 to C.A.S. and B.L.d.G.), the Deutsche Forschungsgesellschaft (Sonderforschungsbereich 803 to R.B. and B.L.d.G.), and the National Institutes of Health (Grant EY015107 to T.W.). A.D.S. is supported by a Swiss National Science Foundation fellowship. T.W. is a Howard Hughes Medical Institute investigator.

1. Marsh D (2008) Protein modulation of lipids, and vice-versa, in membranes. *Biochim Biophys Acta* 1778:1545–1575.
2. Dowhan W, Bogdanov M (2009) Lipid-dependent membrane protein topogenesis. *Annu Rev Biochem* 78:515–540.
3. Dalbey R, Wang P, Kuhn A (2011) Assembly of bacterial inner membrane proteins. *Annu Rev Biochem* 80:161–187.
4. Raja M (2011) The potassium channel KcsA: A model protein in studying membrane protein oligomerization and stability of oligomeric assembly? *Arch Biochem Biophys* 510(1):1–10.
5. Vitrac H, Bogdanov M, Heacock P, Dowhan W (2011) Lipids and topological rules of membrane protein assembly: Balance between long and short range lipid–protein interactions. *J Biol Chem* 286:15182–15194.
6. Phillips R, Ursell T, Wiggins P, Sens P (2009) Emerging roles for lipids in shaping membrane-protein function. *Nature* 459:379–385.
7. Lee AG (2011) Biological membranes: The importance of molecular detail. *Trends Biochem Sci* 36:493–500.
8. Brogden KA (2005) Antimicrobial peptides: Pore formers or metabolic inhibitors in bacteria? *Nat Rev Microbiol* 3:238–250.
9. Jahn R, Scheller RH (2006) SNAREs-engines for membrane fusion. *Nat Rev Mol Cell Biol* 7:631–643.
10. Graham TR, Kozlov MM (2010) Interplay of proteins and lipids in generating membrane curvature. *Curr Opin Cell Biol* 22:430–436.
11. Qualmann B, Koch D, Kessels MM (2011) Let's go bananas: Revisiting the endocytic BAR code. *EMBO J* 30:3501–3515.
12. Marsh D (2010) Electron spin resonance in membrane research: Protein-lipid interactions from challenging beginnings to state of the art. *Eur Biophys J* 39:513–525.
13. Lange C, Nett JH, Trumpower BL, Hunte C (2001) Specific roles of protein-phospholipid interactions in the yeast cytochrome bc1 complex structure. *EMBO J* 20:6591–6600.
14. Murata T, Yamato I, Kakinuma Y, Leslie AGW, Walker JE (2005) Structure of the rotor of the V-Type Na^+-ATPase from Enterococcus hirae. *Science* 308:654–659.
15. Long SB, Tao X, Campbell EB, MacKinnon R (2007) Atomic structure of a voltage-dependent K^+ channel in a lipid membrane-like environment. *Nature* 450:376–382.
16. Shinzawa-Itoh K, et al. (2007) Structures and physiological roles of 13 integral lipids of bovine heart cytochrome c oxidase. *EMBO J* 26:1713–1725.
17. Hunte C, Richers S (2008) Lipids and membrane protein structures. *Curr Opin Struct Biol* 18:406–411.
18. Mitsuoka K, et al. (1999) The structure of bacteriorhodopsin at 3.0 Å resolution based on electron crystallography: Implication of the charge distribution. *J Mol Biol* 286:861–882.
19. Gonen T, et al. (2005) Lipid–protein interactions in double-layered two-dimensional AQP0 crystals. *Nature* 438:633–638.
20. Hite RK, Li Z, Walz T (2010) Principles of membrane protein interactions with annular lipids deduced from aquaporin-0 2D crystals. *EMBO J* 29:1652–1658.
21. Lindahl E, Sansom MSP (2008) Membrane proteins: Molecular dynamics simulations. *Curr Opin Struct Biol* 18:425–431.
22. Marrink SJ, de Vries AH, Tieleman DP (2009) Lipids on the move: Simulations of membrane pores, domains, stalks and curves. *Biochim Biophys Acta* 1788:149–168.
23. Gonen T, Sliz P, Kistler J, Cheng Y, Walz T (2004) Aquaporin-0 membrane junctions reveal the structure of a closed water pore. *Nature* 429:193–197.
24. Hite RK, Raunser S, Walz T (2007) Revival of electron crystallography. *Curr Opin Struct Biol* 17:389–395.
25. Raunser S, Walz T (2009) Electron crystallography as a technique to study the structure on membrane proteins in a lipidic environment. *Annu Rev Biophys* 38:89–105.
26. Schenk AD, Hite RK, Engel A, Fujiyoshi Y, Walz T (2010) Electron crystallography and aquaporins. *Methods Enzymol* 483:91–119.
27. Hite R, Gonen T, Harrison S, Walz T (2008) Interactions of lipids with aquaporin-0 and other membrane proteins. *Pflügers Arch* 456:651–661.
28. Fujiyoshi Y, Unwin N (2008) Electron crystallography of proteins in membranes. *Curr Opin Struct Biol* 18:587–592.
29. Palsdottir H, Hunte C (2004) Lipids in membrane protein structures. *Biochim Biophys Acta Biomembr* 1666:2–18.
30. Ash WL (2009) Helix-helix interactions in membrane proteins probed with computer simulations. PhD thesis, http://hdl.handle.net/1880/48166 (University of Calgary, Alberta, Canada), pp 164–170.
31. Niemelä PS, et al. (2010) Membrane proteins diffuse as dynamic complexes with lipids. *J Am Chem Soc* 132:7574–7575.
32. Spoel DVD, et al. (2005) GROMACS: Fast, flexible, and free. *J Comput Chem* 26:1701–1718.
33. Hess B, Kutzner C, van der Spoel D, Lindahl E (2008) GROMACS 4: Algorithms for highly efficient, load-balanced, and scalable molecular simulation. *J Chem Theory Comput* 4:435–447.